Short term depression, presynaptic inhibition and local neuron diversity play key functional roles in the insect antennal lobe

Kuo-Wei Kao & Chung-Chuan Lo

Journal of Computational Neuroscience

ISSN 0929-5313
Volume 48
Number 2

J Comput Neurosci (2020) 48:213-227
DOI 10.1007/s10827-020-00747-4

Springer

Journal of Computational Neuroscience (2020) 48:213–227
https://doi.org/10.1007/s10827-020-00747-4

Short term depression, presynaptic inhibition and local neuron diversity play key functional roles in the insect antennal lobe

Kuo-Wei Kao[1] · Chung-Chuan Lo[1]

Received: 27 May 2019 / Revised: 13 March 2020 / Accepted: 17 April 2020 / Published online: 9 May 2020

Abstract

As the oldest, but least understood sensory system in evolution, the olfactory system represents one of the most challenging research targets in sensory neurobiology. Although a large number of computational models of the olfactory system have been proposed, they do not account for the diversity in physiology, connectivity of local neurons, and several recent discoveries in the insect antennal lobe, a major olfactory organ in insects. Recent studies revealed that the response of some projection neurons were reduced by application of a GABA antagonist, and that insects are sensitive to odor pulse frequency. To account for these observations, we propose a spiking neural circuit model of the insect antennal lobe. Based on recent anatomical and physiological studies, we included three sub-types of local neurons as well as synaptic short-term depression (STD) in the model and showed that the interaction between STD and local neurons resulted in frequency-sensitive responses. We further discovered that the unexpected response of the projection neurons to the GABA antagonist is the result of complex interactions between STD and presynaptic inhibition, which is required for enhancing sensitivity to odor stimuli. Finally, we found that odor discrimination is improved if the innervation of the local neurons in the glomeruli follows a specific pattern. Our findings suggest that STD, presynaptic inhibition and diverse physiology and connectivity of local neurons are not independent properties, but they interact to play key roles in the function of antennal lobes.

Keywords Local neuron · Olfactory · Computational

1 Introduction

The antennal lobe (AL) receives signals from the olfactory receptor neurons (ORNs) on the antennae. Each type of ORN expresses a single type of olfactory receptor and projects to one of many glomeruli in the AL. Neural signals are picked up by glomerulus-specific projection neurons (PNs) and sent to higher brain regions, including the mushroom body and the lateral horn (Hansson and Anton, 2000; Stocker et al. 1990; Jefferis et al. 2001). Although each of the ORN-glomerulus-PN pathways carries signals from one olfactory receptor type, the neural signals in each glomerulus are not completely independent. Glomeruli are connected by local neurons (LNs), and recent studies have demonstrated diversity in LNs, both in their physiology (Shang et al. 2007; Seki et al. 2010; Assisi et al. 2012) and innervation patterns (Chou et al. 2010; Reisenman et al. 2011). However, some of these findings were not addressed or considered in previous models. While some theoretical studies suggest that LNs enhance odor response contrast (Cleland and Sethupathy 2006; Linster and Cleland 2010; Cleland and Linster 2012; Yu et al. 2014), other studies uncovered a more broad olfactory response in PNs (Bhandawat et al. 2007; Olsen et al. 2007; Shang et al. 2007; Huang et al. 2010).

Neurons in the AL exhibit complex firing activity. In the *Drosophila* AL, ORNs fire spontaneously, without odor input (de Bruyne et al. 1999a, 2001). Short-term synaptic depression in ORNs-to-PNs connections has been observed (Kazama and Wilson 2008) and suggested to be involved in the saturation of PN activity under strong odor inputs. (Rangan 2012). Moreover, most inhibitory LNs respond to odor onsets, while others respond to offsets (Nagel and Wilson 2016). Some LNs also exhibit spontaneous activity and stop firing upon odorant stimulation (Chou et al. 2010; Nagel et al. 2015; Nagel and Wilson 2016).

Action Editor: Albert Compte

Electronic supplementary material The online version of this article (https://doi.org/10.1007/s10827-020-00747-4) contains supplementary material, which is available to authorized users.

✉ Chung-Chuan Lo
cclo@mx.nthu.edu.tw

[1] Institute of Systems Neuroscience, National Tsing Hua University, Hsinchu 30013, Taiwan

The complex behavior and diverse innervation patterns of LNs are believed to be correlated with their function. Previous modeling studies have suggested that the balance between inhibitory and excitatory AL LNs enhances decorrelation of responses to similar odors (Assisi et al. 2012; Shlizerman et al. 2014). Moreover, although odor source locating is believed to be dependent on odor concentration discrimination (Johnson and Leon, 2000; Rospars et al., 2000; Hinterwirth et al., 2004; Yoshida et al., 2012; Zhou and Belluscio, 2012; Arnson and Holy, 2013; Gautam et al., 2014; Hellwig and Tichy, 2016), intermittent odor stimuli caused by odor plumes were also found to provide crucial information for odor source localization (Celani et al., 2014; Justus et al., 2002; Shraiman and Siggia, 2000; Murlis et al. 1992). Previous studies indicated that odor intermittency is a spatial-temporal cue for animals (Park et al. 2014, 2016; Huston et al. 2015).

A recent study showed that the frequency of floral plumes increased, and the intermittency decreased, with increasing distance from the flower (Riffell et al. 2014), and that odor navigation and feeding are significantly decreased by increasing inter-stimulus pulse frequency. The same study also demonstrated that addition of a $GABA_B$ receptor antagonist (CGP54626) led to reduced PN response and decreased odor recognition. These results imply that inhibitory LNs participate in odor plume-associated odor perception.

In this study, we attempted to link the behavior and innervation patterns of LNs to their functions. Specifically, we constructed a spiking neural network model of the insect AL and demonstrated how interactions between ORNs, short-term depression, and spontaneous LNs contribute to odor pulse frequency discrimination, and how these interactions underlie the opposing responses to GABA antagonists. We further showed that the innervation patterns of LNs modulate the ability to discriminate between similar odors and broadens the response of PNs to odor stimuli.

2 Materials and methods

2.1 Network structure

We constructed a scaled-down model of the AL, which contains 10 glomeruli. Each glomerulus is innervated by an ORN, which makes a direct connection with a PN, and by the three observed LN types: spontaneous local neurons (SLNs), passive local neurons (PLNs), and excitatory local neurons (PLNs) (Fig. 1a). SLNs fire spontaneously, without stimulus, and are turned off by the onset of an odor stimulus (Chou et al. 2010; Nagel et al. 2015; Nagel and Wilson 2016). PLNs, in contrast, only fire when there is an odor stimulus, and are the most commonly described inhibitory LN type. ELNs have an activity pattern similar to that of PLNs, but are excitatory local neurons (Olsen et al. 2007; Shang et al. 2007; Huang et al.

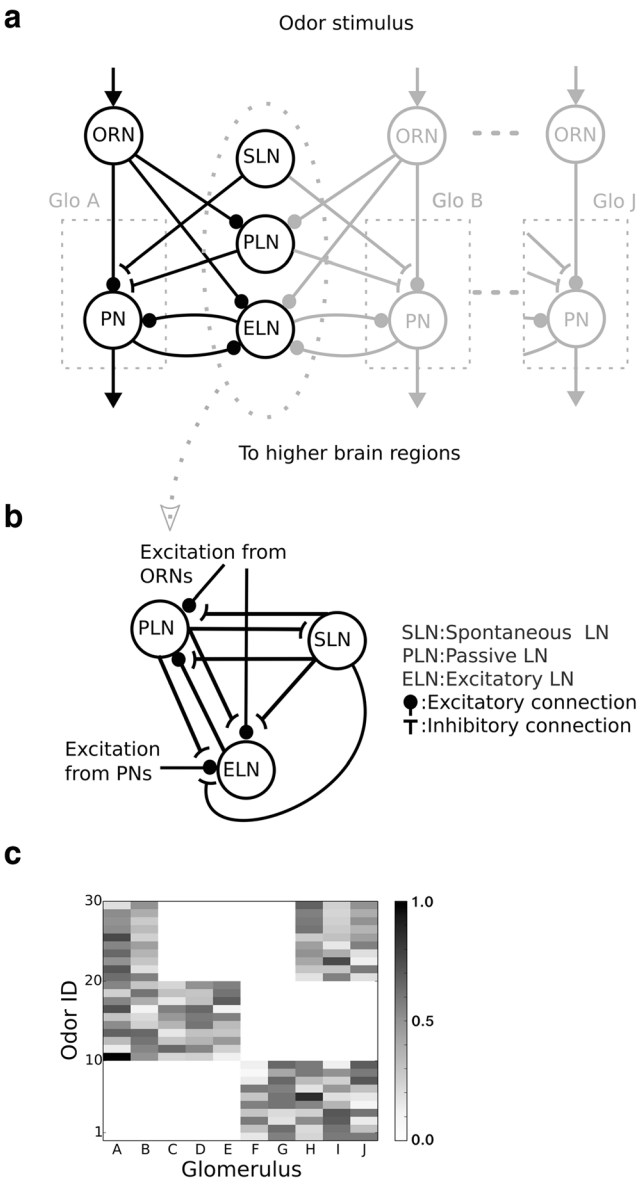

Fig. 1 Schematics of the antennal lobe circuit model. **a** The inter-glomerulus circuit diagram. The model consists of 10 glomeruli (Glo, indicated by dashed boxes), which are identical in structure. Each glomerulus receives input from the olfactory receptor neurons (ORNs), which make synaptic connections with the projection neurons (PNs). Glomeruli are interconnected *via* local neurons (LNs) that are physiologically and anatomically diverse. For visual clarity, we omitted the connections between local neurons, which are depicted in panel B. **b** Connections between local neurons. We simulated three types of local neurons, spontaneous LNs (SLNs), passively LNs (PLNs), and excitatory LNs (ELNs). SLNs and PLNs are inhibitory. All inhibitory connections in the model circuit are pre-synaptic, except for the connections from PLNs to SLNs as this connection suppresses the spontaneous activity of SLNs, rather than blocking the excitatory input as in other LNs. ELNs receive excitatory input from PNs as previously observed (Olsen et al. 2007; Shang et al. 2007). **c** Activation patterns for the 30 artificial odors, which are classified into three groups. Odors in the same group activate the same set of ORNs/glomeruli with different normalized peak firing rates (indicated by the grayscale of each bar), and, therefore, are considered as similar. The odor discrimination task was conducted using odors within the same group

2010; Assisi et al. 2012; Shlizerman et al. 2014)]. The synaptic weights of these LNs were considered as free parameters and were used to fit the model's behavior to the observed effects of the GABA antagonist (Olsen et al. 2010; Riffell et al. 2014) and the odor pulse frequency (Riffell et al. 2014). Since the detailed connectivity between different types of neurons in each insect glomerulus is still not clear, in the proposed model we keep the connectivity as general as possible; nearly every type of LN makes synaptic connections with every other type of neurons (Fig. 1b). The detailed connectivity is described below.

2.2 Artificial odor stimuli

To test how the model circuit responded to different odor stimuli, we generated three groups of artificial odors with each group containing 10 odors. Odors in each group are assumed to be perceptually similar, and they stimulate the same subgroup of ORNs (Fig. 1c). Since a *Drosophila* ORN fires 8 spikes/s in the absence of an odor, on average (de Bruyne et al. 1999b, 2001; Wilson 2013), all ORNs in our model received randomly generated background stimuli to reproduce the observed baseline activity. Each odor input can be described as a 10 dimensional vector, and each dimension corresponds to the input strength to an ORN. To exclude the effects of other unrelated factors, we placed several constraints on the artificial odors: 1) The total input strength (summation of input firing rate across all ORNs) of each odor is a constant, 2) odors in the same group only stimulate the same five glomeruli, and 3) the distance between each normalized odor vector in the same group is set to be 0.3. The purpose of the third constraint is to prevent odors in the same group from being too similar. We created one million odors of the same group following the first two constraints and discovered that the average distance between arbitrary pairs of normalized odor vectors was 0.25. Therefore, the constraint of 0.3 guaranteed that odors in the same group were similar but still distinguishable.

Studies have shown that ORNs adapt to odor stimuli with decaying responses following the odor onset (Wilson 2013). However, the leaky integrate-and-fire model used in the present study does not exhibit input adaptation. To reproduce this property, we set an exponential decay for the odor input. Specifically, the input firing rate of the odor stimulus decayed exponentially to 75% of the initial value with a time constant of 110 ms. This decaying odor input gave rise to an ORN response that resembled observed input adaptation.

For all simulations in our study, the difference between the baseline activity and the peak PN firing rates during odor stimulation were used to represent the neural responses of the model to the odor stimuli. Concentration of an odor is represented by the strength of the odor stimulation.

2.3 Local neurons innervation patterns

We modeled three LN types in each glomerulus: PLNs, ELNs, and SLNs. We tested different innervation patterns for PLNs and ELNs. The default pattern for PNLs and ELNs was assumed to be correlated with long-term odor stimulation. In other words, each PLN and ELN innervated a subgroup of glomeruli stimulated by a specific odor group (Fig. 1c). To this end, we created three groups of LNs with each group containing three PLNs and ELNs. Each group of LNs strongly innervates the glomeruli stimulated by one of the three odor groups and weakly innervates other glomeruli. The default innervation strengths of SLNs in each glomerulus are proportional to the spontaneous firing rate of the ORN innervating that glomerulus. When testing how the LN innervation pattern influences odor discrimination, the targeted LN type follows the innervation patterns stated above and the other LN types use randomly generated innervation patterns. The innervation strength of each LN in each glomerulus is listed in Table 1. There is a total of 9 PLNs, 9 ELNs, and 18 SLNs in the model circuit. The total number of LNs is 36, which is 3–4 times larger than the number of the glomeruli. This ratio is consistence with various observations of fruit fly antennal lobes (Chou et al. 2010; Seki et al. 2010).

2.4 Neuron and synaptic models

2.4.1 Leaky integrate-and-fire neurons

Each neuron in the circuit model is simulated using the leaky integrate-and-fire model. The membrane potential, $V(t)$, for each neuron obeys the following equation:

$$C_m \frac{dV(t)}{dt} = -g_L(\mathrm{V}(t)-V_L)-I_{AHP}-I_{input}, \quad (1)$$

where C_m is the membrane capacitance, g_L is the leak conductance, V_L is the resting potential, I_{AHP} is the current contributed by afterhyperpolarization, and I_{input} is the current produced by external inputs. Both currents are described in detail below. When the membrane potential, $V(t)$, of each neuron reaches a threshold, $V_{threshold}$, a spike is emitted and $V(t)$ is set to the reset potential, V_{reset}. The membrane parameters in our model were set based on previous research (Seki et al. 2010, Gouwens and Wilson, 2009), and adjusted by tuning the values to reproduce the results of previous studies (Olsen et al. 2010; Riffell et al. 2014), as discussed in the subsection "Parameter tuning" below (Table 2). The input current, I_{input}, includes olfactory inputs from odor stimuli; synaptic inputs, I_{syn}, from other neurons in the circuit; and the background input, which is used to generate spontaneous activity in ORNs and SLNs. Odor stimuli were only applied to ORNs.

Table 1 Innervation strength (A) and synaptic efficacy (B) of the proposed network model

A											
Glomeruli		A	B	C	D	E	F	G	H	I	J
ORN		1	1	1	1	1	1	1	1	1	1
PN		1	1	1	1	1	1	1	1	1	1
PLNs, ELNS	#1	0.5	0.5	0.5	0.5	0.5	1.3	1.6	1.4	1.6	1.4
	#2	0.5	0.5	0.5	0.5	0.5	1.3	1.6	1.4	1.6	1.4
	#3	0.5	0.5	0.5	0.5	0.5	1.3	1.6	1.4	1.6	1.4
	#4	1.6	1.5	1.3	1.5	1.4	0.5	0.5	0.5	0.5	0.5
	#5	1.6	1.5	1.3	1.5	1.4	0.5	0.5	0.5	0.5	0.5
	#6	1.6	1.5	1.3	1.5	1.4	0.5	0.5	0.5	0.5	0.5
	#7	1.8	1.3	0.5	0.5	0.5	0.5	0.5	1.5	1.3	1.3
	#8	1.8	1.3	0.5	0.5	0.5	0.5	0.5	1.5	1.3	1.3
	#9	1.8	1.3	0.5	0.5	0.5	0.5	0.5	1.5	1.3	1.3
SLNs	1 ~ 18	0.98	0.75	0.33	0.42	0.38	0.3	0.47	0.84	0.77	0.76
B											
$p_{ORN,\ PLN}$						0.7					
$p_{ORN,\ ELN}$						1					
$p_{PLN,\ ELN}$						0.65					
$p_{ELN,\ PLN}$						0.001					
$p_{ELN,\ PLN}$						0.01					
$p_{PLN,\ SLN}$ for $GABA_A$						0.1					
$p_{PLN,\ SLN}$ for $GABA_B$						0.0002					
$p_{PLN,\ ORN\ (on\ ORN \rightarrow PN\ presynapse)}$ for $GABA_A$						0.25					
$p_{PLN,\ ORN\ (on\ ORN \rightarrow PN\ presynapse)}$ for $GABA_B$						0.00005					
$p_{SLN,\ ORN\ (on\ ORN \rightarrow PN\ presynapse)}$ for $GABA_A$						1					
$p_{SLN,\ ORN\ (on\ ORN \rightarrow PN\ presynapse)}$ for $GABA_B$						0.0001					

2.4.2 Conductance-based synapses

The synaptic input was modeled as change of conductance on the membrane due to activation of receptors at the synapses. We modeled three types of receptors: Ach (cholinergic), $GABA_A$ and $GABA_B$. The synaptic input, I_{syn}, from the presynaptic neuron, i, to the postsynaptic neuron, j, is described by:

$$\begin{aligned} I_{syn} &= g_{Ach,ij} w_{ij} s_{Ach,ij}(t)(V_i(t) - V_E) \\ &+ g_{GABA_A,ij} w_{ij} s_{GABA_A,ij}(t)(V_i(t) - V_I) \\ &+ g_{GABA_B,ij} w_{ij} s_{GABA_B,ij}(t)(V_i(t) - V_I), \end{aligned} \tag{2}$$

where g_r and s_r are the conductance and gating variable for the receptor, r, respectively. w_{ij} is a weight factor modulated by presynaptic inhibition and short-term depression as described below. $V_E\,(=0\ mV)$ and $V_I\,(=-60 mV)$ are reversal potentials for excitatory (Ach) and inhibitory synapses ($GABA_A$ and $GABA_B$), respectively. For each type of the receptor, the gating variable is given by:

$$\frac{ds_{r,ij}}{dt} = -\frac{s_{r,ij}}{\tau_r} + \sum_l \delta\left(t - t_{l,i}\right), \tag{3}$$

where τ_r is the time constant of the receptor r (20 ms for Ach, 5 ms for $GABA_A$, 100 ms for $GABA_B$); t_l is the time of the l-th presynaptic spike; and δ is a Dirac delta function, which is infinity at the time of every presynaptic spike ($t = t_{l,\ i}$) and 0 elsewhere. The total area under the curve of Dirac delta function is 1.

Table 2 Note: This data is mandatory. Please provide

	ORN	PN	PLN	ELN	SLN
Capacitance	0.052 nF	0.007 nF	0.12 nF	0.25 nF	0.005 nF
Refractory Period	3 ms	3 ms	3 ms	3 ms	3 ms
Reset Potential	-52mv	-61mv	-75mv	-75mv	-25mv
Resting Potential	-70mv	-70mv	-70mv	-70mv	-48mv
Membrane Time Constant	16 ms	16 ms	20 ms	20 ms	20 ms
Threshold Voltage	-50mv	-60mv	-50mv	-25mv	−22.2mv

2.4.3 Presynaptic inhibition

We also modeled presynaptic inhibition, which was observed in the fruit fly antennal lobes (Olsen and Wilson 2008). In this type of inhibition, a GABAergic neuron, k, targets the presynaptic terminal of a synapse formed by a presynaptic neuron, i, and a postsynaptic neuron, j. The release of GABA neurotransmitters from the neuron k activates the GABAergic receptors on the presynaptic terminals of the neuron i. The activation triggers an influx of Cl^- which reduces the calcium concentration in the presynaptic terminal, leading to a reduction of presynaptic vesicle release. As a result, the synaptic efficacy decreases (Wu and Saggau 1994; Ohliger-Frerking et al. 2003; Sun et al. 2006; Olsen and Wilson 2008). The effect of presynaptic inhibition is described by the variable $\alpha_{r,k}$:

$$\frac{d\alpha_{r,k}}{dt} = \frac{-\alpha_{r,k}}{\tau_r} + g_{r,ki}\sum_l \delta\left(t-t_{l,k}\right), \tag{4}$$

where the subscript r indicates the target receptor, τ_r is the time constant of the variable α for the receptor r, $g_{r,ki}$ is the synaptic conductance between neurons k and i for the receptor r, and $t_{l,k}$ is the time of the l-th spikes of the neuron k. The time scale of the presynaptic inhibition is dominated by the dynamics of the targeted GABAergic receptors on the presynaptic neuron i. Therefore, we used $GABA_A$'s (τ_r=5 ms) and $GABA_B$'s (τ_r=100 ms) time constants for τ_r in Eq. (4). The normalized calcium concentration, $[Ca_{ij}]$, at the presynaptic terminal of the neuron i is modulated by α_k in the following way:

$$\left[Ca_{ij}\right] = 1-\sum_{r,k}\alpha_{r,k}, \tag{5}$$

where $[Ca_{ij}]$ is limited between 0 and 1.

2.4.4 Short-term-depression

Additionally, we modeled short-term-depression (STD), which describes the reduction of available vesicles following each presynaptic spike and the recovery of the vesicles with a long time constant (Abbott et al. 1997; Varela et al. 1997; Hempel et al. 2000). The effect of STD is described by the variable D, given by:

$$\frac{dD_i}{dt} = \frac{(1-D_i)}{\tau_D} - D_i(1-p_v)\sum_l \delta\left(t-t_{l,i}\right), \tag{6}$$

where τ_D is the time constant of STD, and p_v is the probability of synapse vesicle release (Wang 1999). In our model, $p_v = 0.5$ and $\tau_D = 450$ms. $t_{l,i}$ is the time of l-th spikes of the neuron i. A previous study revealed that the field excitatory postsynaptic potential is proportional to the presynaptic calcium concentration to the power of 3.5 (Wu and Saggau 1994, 1997). Putting both factors together, the synaptic weight, w_{ij} between neurons i and j is modulated by presynaptic inhibition and STD in the following form:

$$w_{ij} = \left[Ca_{ij}\right]^{3.5} D_i. \tag{7}$$

We noted that the power of 3.5 is obtained from the mammalian neurons and the actual power for the insects may be different. Therefore, we tested our model by changing the power to 3.0 and 4.0. We found that the model behavior was insensitive to the exact value of the power, and the overall dynamics and the performance of the model still remained the same (Fig. S1).

2.4.5 Afterhyperpolarization

The afterhyperpolarization was applied to all three local neuronal types based on a previous study (Seki et al. 2010). The afterhyperpolarization (AHP) current IAHP is given by:

$$I_{AHP} = [Ca]_s g_{AHP}(V_m - V_k), \tag{8}$$

where g_{AHP} is the conductance that determines the magnitude of the afterhyperpolarization current and V_k (= − 85 mV) is the reversal potential for potassium channels. g_{AHP} is equal to 2.5 nS for PLNs, 0.4 nS for ELNs, and 0.01 nS for SLNs, which experience almost no AHP as they have a high spontaneous firing rate and a strong AHP would shut the neurons down. $[Ca]_s$ is the calcium centration at the soma, which increases following a spike and decays exponentially afterwards:

$$\frac{d[Ca]_s}{dt} = -\frac{[Ca]_s}{\tau_{AHP}} + \sum_l \alpha_{AHP}\delta\left(t-t_{l,i}\right), \tag{9}$$

where τ_{AHP} (300 ms for PLN, 200 ms for ELN, and 50 ms for SLN) is the time constant of the decay of the somatic calcium concentration, and α_{AHP} (equal to 0.5) determines the magnitude of $[Ca]_s$ increase following each spike.

2.4.6 The synaptic conductance

The synaptic conductance, g_{ij}, between the presynaptic neuron, i, and the postsynaptic neuron, j, is the product of three variables: the innervation strengths, R_i and R_j, and the synaptic efficacy, p_{ij}:

$$g_{ij} = \sum_n R_{in}R_{jn}p_{ij} \tag{10}$$

where R_i represents the innervation strength of i in the glomerulus, n, shown in Table 1A. p_{ij} represents synaptic efficacy, listed in Table 1B. Innervation strength relates to the relative density of neural arbors in a given glomerulus. The product of the innervation strengths of two neurons in said glomerulus gives an estimate of the number of synapses the neurons can form in the glomerulus. Synaptic efficacy indicates the strength of a single synapse. Therefore, the product of R_{in}, R_{jn},and p_{ij} represents the overall synaptic conductance, or the connection

strength between the two neurons. We demonstrate how synaptic conductance is calculated in two following examples.

Example 1: ORN to PLN #1 in glomerulus A.

$$g_{ORN_A,PLN_{\#1}} = R_{ORN_A} \times R_{PLN_{\#1}} \times p_{ORN_A,PLN_{\#1}} = 1 \times 0.5 \times 0.7 = 0.35 \quad (11)$$

Example 2:

The efficacy of the PLN #1 to SLN #1 connection targeting $GABA_A$ receptors. (please refer to Tabel1)

$$g_{PLN_{\#1},SLN_{\#1}} = \sum_{all\ glomeruli} R_{PLN_{\#1}} \times R_{SLN_{\#1}} \times p_{PLN,SLN} \text{ for } GABA_A \quad (12)$$
$$= \Big(1 \times 0.5 \times 0.98 + 1 \times 0.5 \times 0.75 + 1 \times 0.5 \times 0.33 + 1 \times 0.5 \times 0.42 + 1 \times 0.5 \times 0.38 + 1 \times 1.3 \times 0.3 + 1 \times 1.6 \times 0.47 + 1 \times 1.4 \times 0.84 + 1 \times 1.6 \times 0.77 + 1 \times 1.4 \times 0.76\Big) \times 0.1 = 0.6044$$

2.5 Discrimination improvement score

To investigate the role of LNs in odor identity discrimination, we need to compare the neuronal responses of ORNs and PNs to pairs of similar odors. The response of ORNs to an odor could be quantified as a vector in 10 dimensional space, in which each dimension corresponds to the firing rate of an ORN. The Euclidian distance, d_{ORN}, between the vectors of the two odors represents the difference between them. Likewise, we can also quantify the response of PNs to an odor as a vector in 10-dimensional space and measure the Euclidian distance, d_{PN}, between the vectors of the two odors. To measure whether the model circuit discriminates similar odors at the PN level better than at the ORN level, we calculated the discrimination improvement score, defined as $\Delta d = d_{PN} - d_{ORN}$, for each odor pair within the same odor group. A positive Δd indicated that the circuit improved odor discrimination because it was better at the PN levels than at the ORN level, while a negative Δd indicated the opposite. There were 45 odor pair combinations in each group, giving rise to a total of 135 pairs of similar odors in the three groups. To assess how the innervation patterns of LNs influence odor discrimination, we compared Δd's with different types of LN innervation pattern.

2.6 Similar odor discrimination task

In addition to investigating how LNs increase the distance between different odors using the discrimination improvement score as described above, it is important to examine, when taking the intrinsic noise and trial-to-trial variability into account, whether our model circuit still improve discrimination between similar odors. First, we chose an arbitrary odor A and recorded the PN responses to A for 10 trials. Next, we performed another 10 trials with randomly selected odors from the same group (but exclude the odor A). The PN responses to a given odor in one trial can be viewed as a point in a high dimensional space with each dimension representing the response of one PN (Fig. S2). Ideally, the 10 points that corresponded to the 10 trials of odor A would be very close to each other and far away from the other 10 points that corresponded to the 10 trials of different odors. However, due to the noise and variability, there was overlap between the distributions of the two sets of points. To quantify how well the system could separate the two sets of points, we chose an odor A point arbitrarily and set a distance r as the discrimination criterion. Any point that fell within the distance r from this point was classified as odor A, and all other points as not odor A. Next, we calculated the true positive, true negative, false positive and false negative numbers. These four numbers gave us one data point on the ROC (receiver operating characteristic) plot. By varying the distance criterion r (= 10, 20, 30, 40, 50, 60, 70, 80, 90, 100 Hz), we obtained multiple points and plotted a ROC curve. We repeated this procedure ten times and each time we randomly selected an odor as the odor A. Finally, we calculated an averaged ROC curve from the 10 repeats, and we selected the optimal criterion from the averaged ROC curve to make a confusion matrix.

2.7 Odor pulse frequency

Following the observations described in (Riffell et al. 2014), we tested whether the model circuit was sensitive to the odor pulse frequency.,The odor pulse stimulus was simulated as intermittent pulse input to ORNs. For an odor pulse stimulus of x Hertz, the input was turned on every $1/x$ seconds, and turned off $1/2x$ seconds afterwards (Riffell et al. 2014). As a result, the odor stimulus always presented for half of the time, regardless of frequency. As described in the Results section, we found that the response of PNs decayed across consecutive odor pulses. To quantify the decay, we measured the decay rate as follows. First, the peak of PN response during each input pulse was identified. Next, the sequence of peaks over time was fitted by a linear function $y = Ax + B$, where x represented the time of each peak and y was the PN peak firing rate. A and B were the fitting parameters. We defined the absolute value of the slope, A, as the PN peak decay rate.

2.8 Parameter tuning

The proposed model involved a large number of parameters, including the membrane properties of each neuron type, the synaptic strength between connected neurons, and other synaptic properties. We determined these parameters by the following

strategy. We first constructed a simple network containing only one single glomerulus with one neuron of each type. Using this simple network, the synaptic efficacy, p_{ij}; parameters associated with STD and AHP; and membrane properties of all neuron types except ELN were determined by reproducing the effect of odor-pulse-induced response decay (Riffell et al. 2014), and by fitting the input-output curve to an empirical input gain model introduced in a previous study (Olsen et al. 2010):

$$PN = R_{max}\frac{ORN^{1.5}}{ORN^{1.5} + k^{1.5}}, \quad (13)$$

where PN refers to the response of an individual PN to an odor stimulus, and ORN is the individual presynaptic ORN response to the same stimulus. The equation contains two fitting parameters: R_{max} represents the maximum odor-evoked PN response, and k represents the level of ORN input that produces a half-maximum response of the PNs. The power of 1.5 was pre-determined based on a previous study (Olsen et al. 2010).

Finally, the parameters for the ELNs were determined by reproducing the PN response broadening described in previous studies (Hallem and Carlson 2006; Bhandawat et al. 2007; Olsen et al. 2007; Shang et al. 2007; Huang et al. 2010). No synaptic efficacy or membrane parameter was changed when we tested the ability of the network to determine odor distance and discriminate between similar odors.

2.9 Experimental design and statistical analysis

This study consists of four sets of simulated experiments. The method used in calculating the firing rate is described in the Fig. 2 legend. The experimental design of "Odor pulse frequency discrimination" is described in the subsection "Odor pulse frequency" above, and in the legend of Fig. 3. The experimental design of "Response enhancement by the GABA antagonist" is provided in the legend of Fig. 4, and the statistical methods used for analyzing the data can be found in the Results section describing Fig. 4. The experimental design of "Discrimination between similar odors" is described in the subsections "Artificial odor stimuli", "Local Neurons innervation patterns", and "Odors identity discrimination" above. The statistical methods used for analyzing the results are described in the Fig. 5 legend. The experimental design of "PN responses broadening" can be found in the Fig. 6 legend, and the statistical methods used for analyzing the data are provided in the Results section describing Fig. 6.

2.10 Code accessibility

The model source code can be accessed at modelDB, url= http://modeldb.yale.edu/238959.

3 Results

3.1 Model network and neural activities

In the present study, we designed and built a scaled-down network model of the insect AL containing three types of LNs with diverse innervation patterns and short-term depression at the ORN to PN synapses (Fig. 1). We tested the model circuit by stimulating it with randomly generated odor stimuli and found that the general responses of each neuronal type were consistent with the experimental observations (Fig. 2). A large portion of the local neurons (PLNs and ELNs in the model) respond to the odor stimulus, while the spontaneous local neurons (SLN) exhibit the opposite activity pattern.

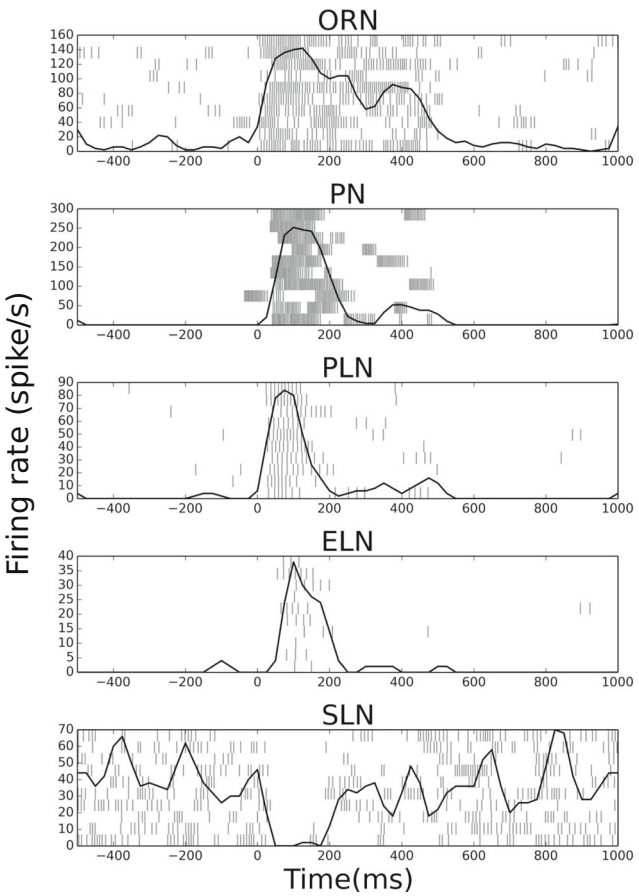

Fig. 2 Representative neural response of the model to an odor stimulus. The spikes raster and average firing rates of all neuron types from one glomerulus (Glomerulus A). The model circuit was stimulated by the odor #1 in the odor map (Fig. 1c), for t = 500 ms. The activity of each neuron type for 10 repeated trials is shown. Each vertical tick represents one spike, and each row of ticks displays the spike activity in one trial. Curves indicate the average firing rate from the 10 trials shown. Most neurons exhibited transient responses to the odor stimulus, except for SLN, which exhibited spontaneous activity, which paused when the odor was presented. Firing rates are calculated by using a sliding window with a size of 50 ms and a time step of 25 ms

3.2 Odor pulse frequency dependent responses

The proposed model was able to produce frequency-dependent responses to odor pulses, an observation that was suggested to be related to the ability of moths to locate the odor source (Riffell et al. 2014). We delivered the odor stimulus in the form of repetitive pulses of different frequencies (from 1 Hz to 10 Hz) and observed that PNs responded with bursts of activity matched the time-course of the stimuli (Fig. 3a). We further observed that peak responses were weaker for higher frequency stimuli and that peak heights decay with time. Interestingly, the peak height decay rate, as measured by the slope of peak firing rate *versus* time, increases with odor pulse frequency (Fig. 3b). Standard deviation of fitted coefficients (a and b in the linear equation y = ax+b) in Fig. 3b are: a = −1.01±1.36, b = 46.2±3.33 for 1 Hz, a = −11.9±7.56, b = 39.3±3.70 for 5 Hz, and a = −17.9 ±3.95, b = 37.7±2.11 for 10 Hz.

To test which dynamic property of the model contributed to the frequency-dependent response decay, we measured decay rate under three conditions: removal of

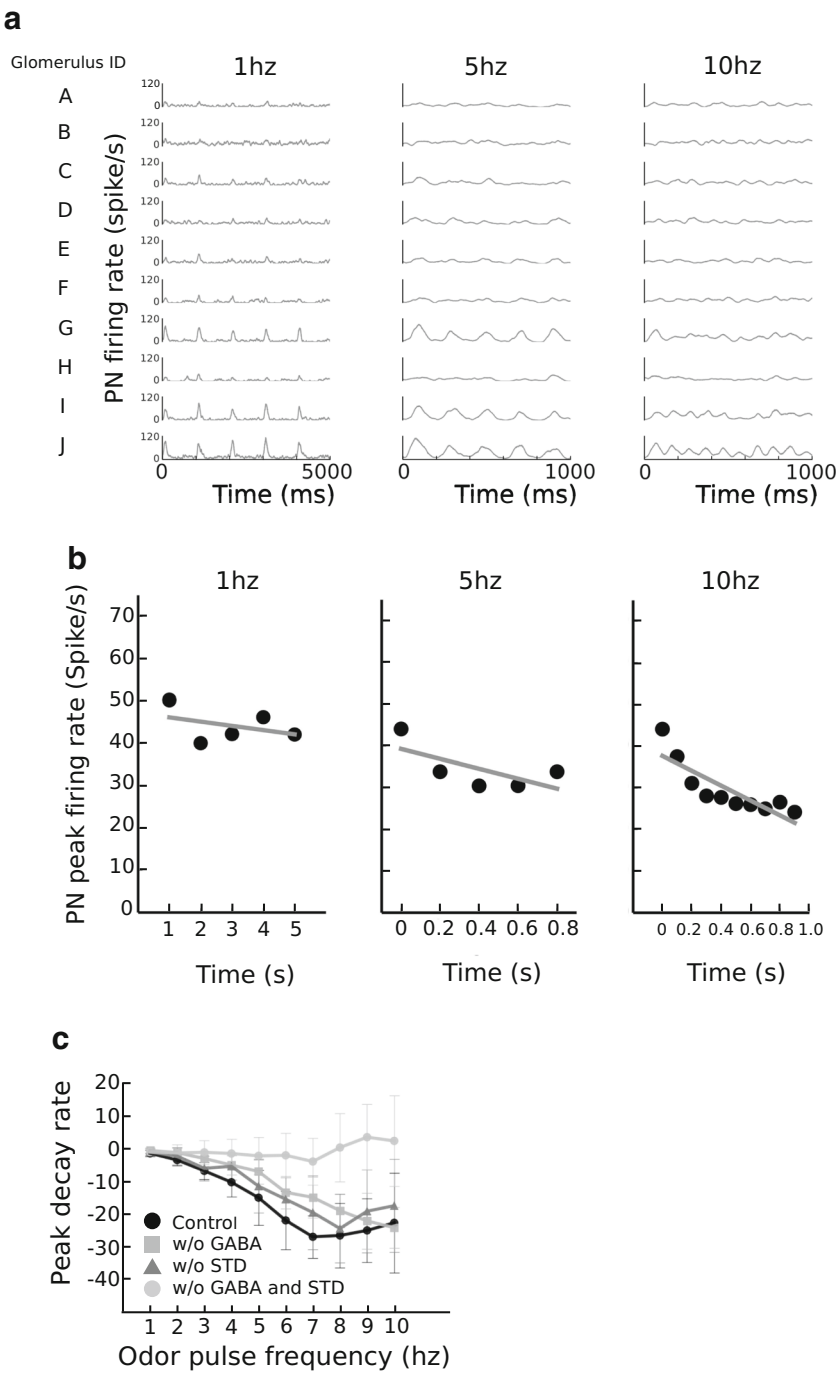

Fig. 3 Odor pulse frequency discrimination by the model circuit. **a** Representative PN responses to the same odor source with different odor pulse frequencies. Each row displays the trial-averaged ($N = 100$) PN firing rate in one glomerulus. **b** PN peak responses, averaged across all glomeruli, to the same odor source (as in panel A) for three different odorant pulse frequencies. Gray lines represent the linear fitting of the data points. **c** Decay rate of PN peak activity, represented by the slope of the line of best fit (shown in B), as a function of odor pulse frequency. In the normal (control) condition (black circles), the absolute value of the decay rate increased with the odor pulse frequency. Removal of GABA synapses (gray stars) or short-term depression (STD) (dark-gray circles) only slightly affected the decay rate. However, the removal of both GABA and STD (light-gray circles) completely abolished the effect. Error bars indicate the standard deviation of the data from 30 odors

GABAergic connections, removal of STD, or both. Our results revealed that while removing either component slightly affected the decay rate, removing both completely abolished frequency-dependent response decay (Fig. 3c). Moreover, this effect is stronger for higher odor frequencies. The results suggested that the interaction between the two components is crucial for the model's ability to discriminate odor pulse frequency.

3.3 Response enhancement by the GABA antagonist

Recent studies in *Drosophila* demonstrated a GABA receptor antagonist reduced the response of some PNs to odor stimuli (Olsen et al. 2010; Riffell et al. 2014), which is in opposition to the expected disinhibition, as inhibitory LNs suppress PN activity *via* presynaptic inhibition (Olsen and Wilson 2008; Okada et al. 2009; Wang 2012). Our model was able to reproduce the diverse responses of LNs upon treatment with a GABA antagonist (Olsen et al. 2010; Riffell et al. 2014; Raccuglia et al. 2016). We measured peak PN activity over 100 trials and calculated the mean as a function of peak ORN activity with or without a GABA antagonist (Fig. 4). To visualize trends, the data were fit by eq. (13) using the non-linear least squares method. We found that PNs, without strong SLN innervation exhibited weaker activity upon treatment with a GABA antagonist than without (Fig. 4c and d). This result is consistent with the idea that GABA antagonists increase neuronal responses due to reduced inhibition. However, we also found that PNs, with strong SLN innervation developed stronger activity upon treatment with a GABA antagonist than without one (Fig. 4a and b), a phenomenon that has been previously observed (Riffell et al. 2014). We further found that the GABA-antagonist-dependent response enhancement was the result of interaction between STD and SLN. This was evident from the distinct availability of presynaptic vesicles, with or without GABA, when strong SLN innervation was present (Fig. 4e). On the other hand, when there was no strong SLN innervation to a glomerulus, no significant difference in the availability of the presynaptic vesicles was observed with or without GABA (Fig. 4f). We discuss the underlying mechanism in detail in the discussion. Each data point shown in Fig. 4 was averaged over 100 trials, and the error bars shown in Fig. 4a and c are the standard error of the mean. To test whether the PN responses are significantly different between the w/ GABA and w/o GABA conditions, we used the paired t-test for each pair of data points. The P values with Bonferroni correction are 1.00, 1.00, 1.00, 1.00, 2.51×10^{-3}, 3.62×10^{-25} and 2.24×10^{-45} (Fig. 4a, from left to right); 8.40×10^{-10}, 5.30×10^{-6}, 1.00, 2.60×10^{-9}, 8.30×10^{-15}, 5.21×10^{-17}, and 1.56×10^{-15} (Fig. 4c from left to right). The mean squared errors for the curve fitting are 142.1 (w/ GABA) and 22.7 (w/o GABA) in Fig. 4a; 94.0 (w/ GABA) and 87.9 (w/o GABA) in Fig. 4c.

3.4 Discrimination between similar odors

In addition to distance discrimination, we also tested how the model network improved discrimination between similar odors, which are represented by similar ORN activation patterns. Based on a previous study (Hallem and Carlson 2006), which demonstrated that odorants containing the same functional groups activate a similar subset of glomeruli, we generated three groups of artificial odors with each group containing 10 odorants that activate the same subset of ORNs with similar normalized peak firing rate (see Methods)(Fig. 1c). As LNs propagate information between glomeruli and modulate PN responses to each odor input, we therefore tested whether the innervation patterns of LNs are critical to odor discrimination. To this end, we calculated the discrimination improvement score of the model with various LNs innervation patterns. We tested random or patterned innervation for each of the three LN types, which gave rise to a total of eight different innervation pattern combinations (Table 3).

We first tested discrimination improvement for PN output and ORN response for the four innervation combinations (Table 3). For each innervation combination, we tested all 135 similar odor pairs and examined the distribution of the discrimination improvement scores. We found that odor discrimination of PN output was better than those of ORNs under all conditions (Fig. 5a), suggesting that the inclusion of LNs always improves odor discrimination, regardless the innervation pattern. The paired t-test result of Fig. 5a: t value = 28.1, p value = 6.71×10^{-137} between patterned PLNs and Random; t value = 28.2, p value = 5.59×10^{-138} between patterned PLNs and patterned ELNs; t value = 30.8, p value = 6.06×10^{-158}between patterned PLNs and patterned SLNs. Next, we compared the difference in discrimination performance between each innervation pattern combination listed in Table 3. Our result showed that the performance of a patterned PLN network is significantly better than that of all other combinations (Fig. 5b, c, d). The mean values of the distributions in Fig. 5b, c, d are significantly different from 0 as verified by one sample t test (t value = −28.1, p value = 6.71×10^{-137} for panel B; t value = −30.8, p value = $6.06 \times 10^{-158}$for panel C; t value = −28.2, p value = 5.59×10^{-138} for panel D.) In conclusion, the innervation pattern of PLNs significantly affects odor discrimination, and this odor-correlated innervation pattern leads to a better performance than random innervation pattern. On the other hand, the innervation pattern of ELNs and SLNs show no significant difference in odor discrimination from that of a random pattern (Fig. 5a).

Due to the intrinsic noise in the neural circuits and the trial-to-trial variability in the input spike trains, the PNs exhibit different responses to the same odor in different trials. Therefore, it is important to ask how such variability affects the ability of the model circuit to discriminate one odor from

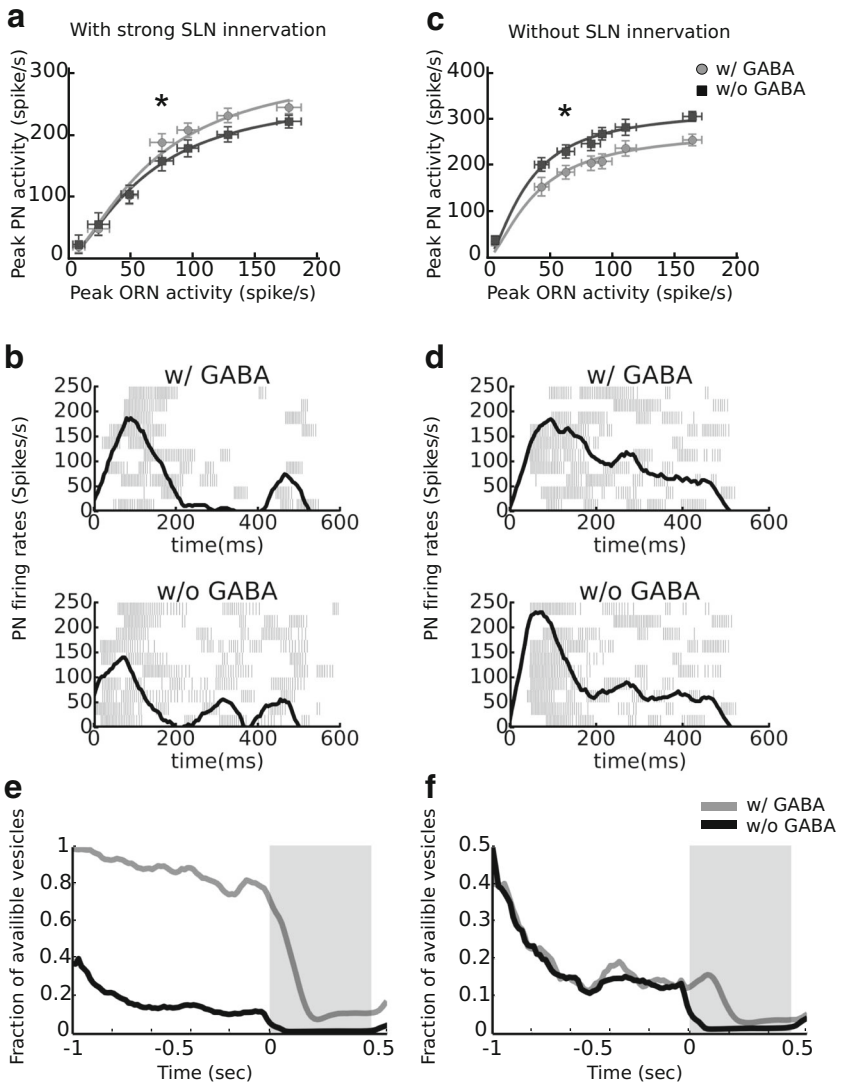

Fig. 4 Simulated GABA antagonist produce diverse PN responses. **a** Peak PN activity as a function of peak ORN activity in a single glomerulus that is strongly innervated by SLN. When all GABAergic connections were turned off (w/o GABA), PN responses were significantly lower than that when the GABAergic connections remained intact (w/ GABA). **b** firing rates (black curves) and spike rasters (ticks) of the trials shown in the panel E. Each row of spike rasters represents a single trial. **c** As in panel A except peak PN activity is for a glomerulus without SLN innervation. When all GABAergic connections were turned off (w/o GABA), PN responses were significantly higher than when GABAergic connections remained intact (w/ GABA). These two glomeruli were stimulated by the same odor, and the innervations of PLNs and ELNs to both glomeruli were randomly assigned. The response of ORNs and PNs to the odor stimuli were transient, so their activities are represented by peak firing rates. The data were fitted by eq. (13) (curves) using the non-linear least square fit. Each data point indicates the mean over 100 trials, and the error bars represent the standard error of the mean. **d** firing rates (black curves) and spike rasters (ticks) of the trials shown in the panel F. Each row of spike rasters represents a single trial. **e** The fraction of available vesicles in the ORN-to-PN synapses, as a function of time, under conditions strong SLN innervation as in panel A. The gray area indicates the period of the odor stimulus. The weaker PN responses in the w/o GABA condition, as indicated in panel A, is the consequence of fewer available presynaptic vesicles before stimulus onset. **f** Same as in panel E except without SLN innervation. The input strengths used in panels E and F are indicated by asterisks in panels A and C, respectively. Firing rates in panels B and D are calculated by using a sliding time window with a size of 50 ms and a time step of 25 ms

other similar odors. To this end, we conducted the similar odor discrimination task (see Methods). We plotted the ROC curves for different LN innervation patterns and calculated the confusion matrices (Fig. 5e and f). We found that, in consistent with the results presented in Fig. 5a–c, the patterned PLNs gave rise to the best discrimination between similar odors.

3.5 PN response broadening

The proposed model also exhibited response broadening as observed in several previous studies (Bhandawat et al. 2007; Olsen et al. 2007; Shang et al. 2007; Huang et al. 2010), which showed in several cases that there are more PNs responding to

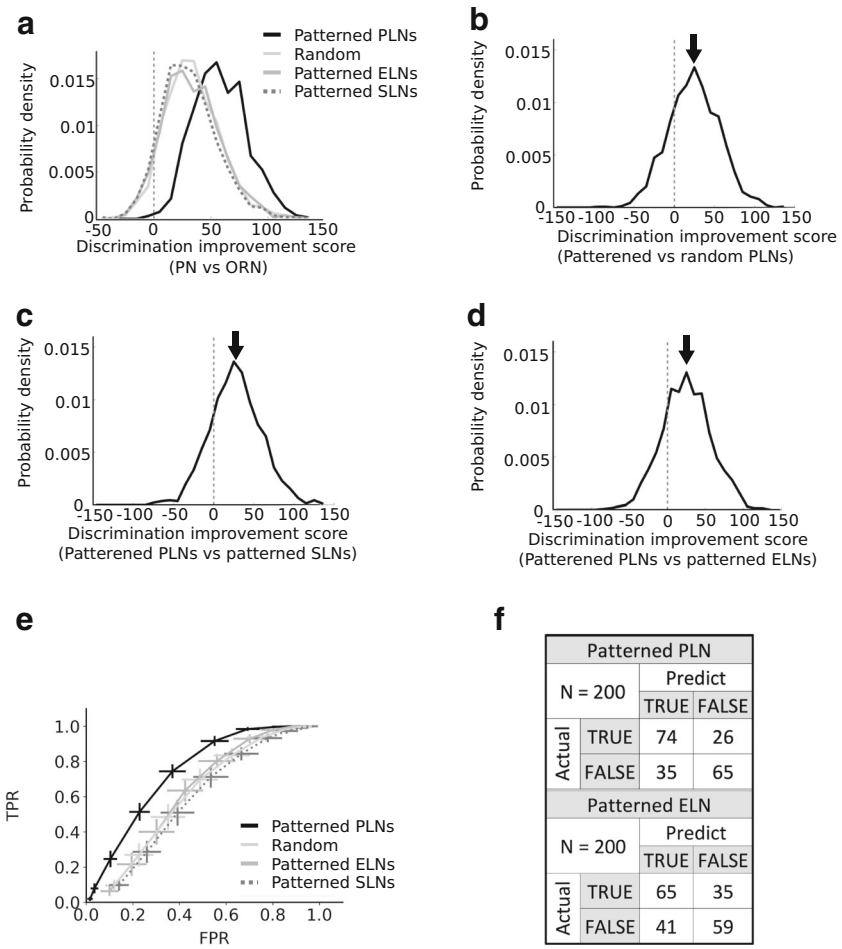

Patterned PLN			
N = 200		Predict	
		TRUE	FALSE
Actual	TRUE	74	26
	FALSE	35	65

Patterned ELN			
N = 200		Predict	
		TRUE	FALSE
Actual	TRUE	65	35
	FALSE	41	59

Fig. 5 Discrimination of similar odors can be significantly improved by patterned PLN distribution. **a** Distribution of discrimination improvement scores for all odor pairs (within in the same group). The discrimination improvement score is measured by the difference in the ability of PN and ORN to discriminate between two given odors (see Methods). A positive value indicates that LNs improve discrimination ability for similar odors. We set the innervation pattern of given LN types (indicated by the legends) to match that of the overall odor activation patterns, and tested how discrimination between similar odor discrimination can be improved. PLNs with patterned innervation produced the greatest improvement in discrimination. **b** Distribution of discrimination improvement scores for all odor pairs (within the same group). We compared networks with patterned PLNs to those with random PNLs. The overall positive score values suggest that the former performs better than the latter. **c** and **d** are similar to (B), but for patterned PLNs compared to patterned SLNs and ELNs, respectively. The vertical dash line indicates 0 discrimination improvement, and the arrow indicates the mean value of distribution. The result suggests that a network with patterned PLNs results in overall better discrimination ability compared to networks with patterned SLNs or ELNs. **e** Receiver operating characteristic (ROC) curves for the similar odor discrimination task. Each curve depicts the true positive rate (TPR) as a function of the false positive rate (FPR) in the task for a given LN innervation pattern. The result indicates that the patterned PLNs gives rise to the best similar odor discrimination. The error bars represent the standard error of the means. **f** The confusion matrices for the optimal discrimination criteria in the similar odor discrimination task for patterned PLNs and patterned ELNs. The optimal criteria were determined by selecting the points that were closest to the upper left corner in the ROC plot from each curve

an odor than ORNs. This phenomenon is not favored by a number of computational models, which suggest response sharpening (or contrast enhancement) for better discrimination (Cleland and Sethupathy 2006; Linster and Cleland 2010; Cleland and Linster 2012). We tested our model by recording ORN and PN responses to all odors, and discovered that all of these odors elicited responses in more PNs than ORNs, examples of which are shown in Fig. 6a. Response broadening can be attributed to the ELNs, which has been reported in several previous studies (Hallem and Carlson 2006; Bhandawat et al. 2007; Olsen et al. 2007; Shang et al. 2007; Silbering and Galizia 2007; Kazama and Wilson 2009; Huang et al. 2010; Shlizerman et al. 2014). The ELNs that are activated by an odor project laterally and excite PNs in glomeruli that do not receive input from the given odor. The degree of broadening can be measured by the effective radius of the response histogram (see Fig. 6a legend). By comparing differences between the effective radius of the network with or without ELNs, we

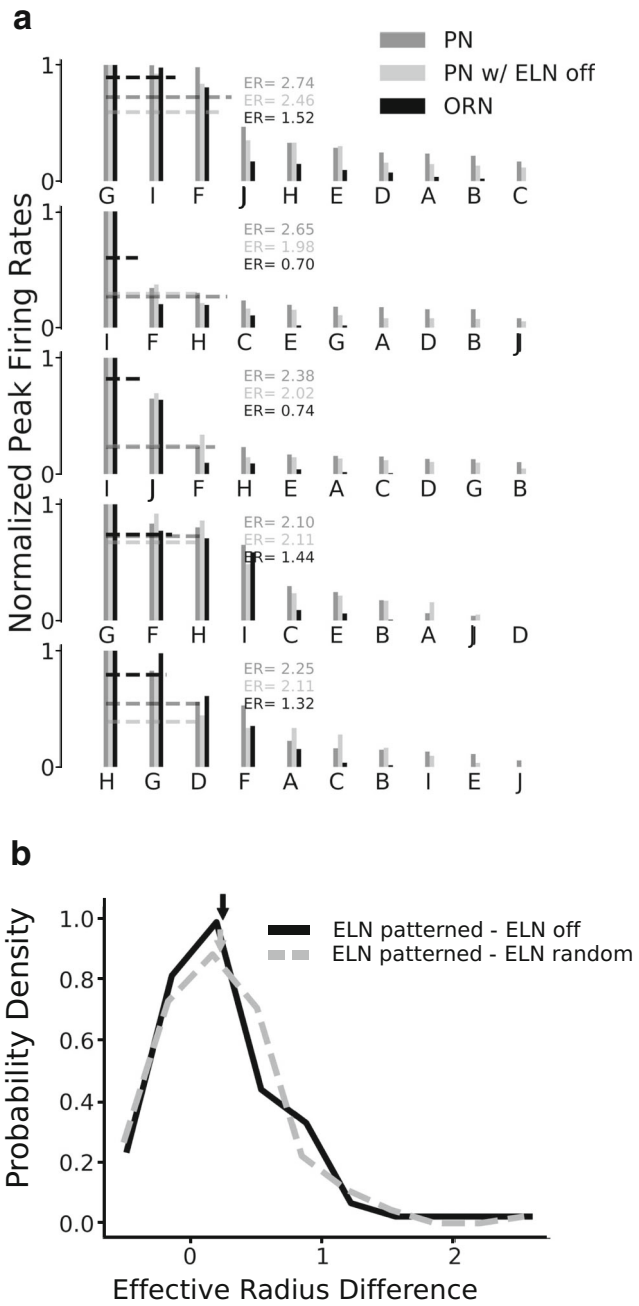

Fig. 6 The model circuit shows broadened PN responses compared to ORN responses. **a** We plot the normalized peak firing rates of ORNs and PNs for all glomeruli (ordered by the firing rate) for five randomly chosen odors. For PNs, the firing rates are plotted for the network with ELNs or without ELNs (w/o ELN). To quantify how the odor responses are broadened at the PN level, we calculate the effective radius (ER) of these histograms. The effective radius, as represented by the dashed lines, is defined as the center of mass with the position x representing the order of the glomeruli as an integer (from 0 to 9) and the mass representing the normalized peak firing rate of the ORNs or PNs in each glomerulus. We saw a response of PNs to odors in glomeruli where ORNs did not respond, indicating a broadened response in PNs as has been previously observed in several studies (Hallem and Carlson 2006; Bhandawat et al. 2007; Olsen et al. 2007; Shang et al. 2007; Huang et al. 2010). **b** The distribution of effective radius differences. To assess the effect of ELNs in response broadening, we calculated the difference in effective radius between networks with or without ELN for each odor, and plotted the distribution of these differences (black). We also show the distribution of the effective radius differences between networks with patterned and random ELN innervations (gray). These results indicate that without patterned ELN innervation, the broadening effect in PNs is reduced. The mean of each distribution is indicated by arrows of the same color

found that the presence of ELNs significantly broadened PN response to the odors (Fig. 6b). We also tested the effect of ELN innervation pattern on PN response broadening by comparing the PN response with patterned or random ELN innervation. We found that patterned ELN innervation induced a broader PN response than that by random ELN innervation (Fig. 6b). The mean values of the distributions in Fig. 6b are significantly different from 0 as verified by one sample t-test (t value = 5.56, p value = $1{,}39 \times 10^{-7}$ for ELN off; t value = 5.64, p value = 9.87×10^{-8} for ELN random.).

Table 3 Note: This data is mandatory. Please provide

	PLNs	ELNs	SLNs
1	Patterned	Random	Random
2	Random	Patterned	Random
3	Random	Random	Patterned
4	Random	Random	Random

4 Discussion

In the present study we proposed a neural circuit model of the insect AL featuring three local neuron types, specific local neuron innervation patterns, and presynaptic short-term depression. Interactions between the three features give rise to complex neuronal responses that resemble several observed characteristics of activity in the insect AL. Our model suggests that these characteristics are not independent of each other, but are correlated due to the underlying neural mechanisms and some functional requirements. We discuss their correlation below.

4.1 Odor pulse frequency dependent response requires STD and presynaptic inhibition

Odorant molecules propagate in a plume-like structure and animals utilize this feature to track the odor sources as well as to determine odor distance (John Murlis et al. 1992; Huston et al. 2015; Riffell et al. 2014). Odor plumes are perceived by the ORNs as intermittent odor stimulations, with a frequency depending on the distance from the odor source (Riffell et al. 2014). We showed that the proposed model is able to turn the intermittent ORN inputs into a decaying PN response as

observed (Riffell et al. 2014), and the decay rate is input frequency dependent.

Our analysis indicated that both STD and GABAergic synapses are crucial for the input frequency dependent decay rate. Interestingly, removing either STD or GABA only produced a slight impact to the frequency dependent decay rate, while removing both completely abolish this effect. The underlying mechanism can be understood through Eq. 7. This equation describes the dynamics of the synaptic weight w, and therefore determines the responses of PN to the odor stimuli. Based on the equation, w is influenced by the presynaptic calcium concentration $[Ca^{2+}]$ (the target of the presynaptic inhibition) and the STD variable D in a multiplicative way. $[Ca^{2+}]$ and D are defined in Eqs. 4–6 and both variables follow similar dynamics: they decay rapidly under high frequency stimuli and slowly under low frequency stimuli (Fig. S3). Therefore, the weight w, as the product of $[Ca^{2+}]^{3.5}$ and D, also follow the same dynamics. If we turn off the dynamics of $[Ca^{2+}]$ by making it a constant, w still maintains the frequency dependent decay rate due to the effect of D. Likewise, turning of STD alone does not produce a large impact on the frequency dependent decay rate in w due to the effect of $[Ca^{2+}]$. Only turning off both would completely abolish such effect. Interestingly, for lower input frequencies, removing $[Ca^{2+}]$ or D produces a nearly linear effect on w, while in the high input frequency regime, the effect of removing $[Ca^{2+}]$ or D is more nonlinear effect on w (Fig. 3d). This, again, is due to the nature of the multiplicative relationship described in Eq. 7.

Note that for the odor stimuli with the same frequency, a stronger stimulus (higher concentration) produces more depletions in $[Ca^{2+}]$ and D, leading to a weaker PN response to the next input pulse, or a larger PN response decay rate. Therefore, the decay rate is roughly proportional to the input amplitude.

4.2 Role of presynaptic inhibition in ORN sensitivity

Inferentially, based on our simulation, a neuron in the resting state is not sensitive to an external stimulus because the neuron can only be excited if the stimulus is stronger than a certain threshold. In contrast, a neuron with a small spontaneous activity is highly sensitive to the stimulus because the firing rate increases for any small input. Indeed, most ORNs have spontaneous activity (de Bruyne et al. 1999a, 2001) and they are highly sensitive to odorant stimuli. However, with the presence of STD, spontaneous activity in ORNs quickly depletes presynaptic vesicles in the ORN-to-PN synapses. As a result, the synapses become highly depressed and the sensitivity of PNs to odorant stimuli is significantly reduced. Our model suggests that SLNs may play a role in resolving this problem. SLNs activate spontaneously when there is no odorant stimulus and they exert presynaptic inhibition on the ORN-to-PN synapses. This inhibition prevents ORNs from releasing synaptic vesicles and therefore no STD is induced. When the system receives an odorant input, activated ORNs excite PLNs, which in turn inhibit SLNs, leading to disinhibition of the ORN-to-PN synapses. The disinhibited synapses can then fully respond to the odorant input until STD kicks in. Without the effect of GABA, ORN-to-PN synapses will become depressed before the odorant input and the frequency-dependent response decay will not occur.

Based on this argument, ORNs with higher levels of spontaneous activity require stronger SLN innervation to suppress the presynaptic activity. This is exactly the setting in our model, and led to inhomogeneous SLN innervation to each glomerulus and produced different responses to a GABA antagonist, as shown in Fig. 4. Each ORN-to-PN synapse receives two sources of GABAergic inputs: SLNs and PLNs. In the synapses without strong SLN innervations, STD is not suppressed and the level of available presynaptic vesicles remains low. In these synapses, the effect of PLNs is dominant, and PLNs reduce PN activity after the odor onset. Adding a GABA antagonist eliminates the effect of PLNs, and therefore PNs exhibit stronger activity than in the condition without the GABA antagonist. On the other hand, in synapses with strong SLN innervations, the effect of SLNs is dominant, and the synapses maintain high levels of available presynaptic vesicles. The addition of a GABA antagonist eliminates the effect of the SLNs and reduces the available vesicles, leading to a weaker PN response after odor onset.

4.3 The innervation pattern of passive local neurons

Our model suggests that PLN innervation patterns correlate with odor activation patterns at the glomerulus level. We would like to emphasize that this model does not exclude the existence of other PLN innervation patterns as they have been found to be highly diverse (Chou et al. 2010). Moreover, this model does not require an "exact" match between the PLN innervation patterns and the odor activation patterns. As described in Table 1A and in Methods, PLNs only need to have stronger synaptic weights in the glomeruli that are strongly activated by a specific odor group. Although the available data is not enough to verify such a conclusion, it is not unreasonable, from the perspectives of neural development, because repetitive stimulation by certain odors may promote growth of local neurons in activated glomeruli during the developmental stages.

The next question is why patterned PLN innervation increase d_{PN} more than other types of LN innervation do? One way to increase d_{PN} is to ensure that PNs develop stronger responses to the odors so that the PN response vectors become longer. ORN-to-PN synapses are inhibited by SLNs, which are, in turn, inhibited by PLN at the onset of an odor stimulus.

Therefore, a strong PN response to an odor requires strong activation of PLNs, which disinhibit ORN-to-PN synapses *via* SLN. A PN can be strongly activated if its innervation to the glomeruli overlaps with those activated by an odor. This explains why the PN innervation pattern, which correlates with the activation pattern of an odor group, can improve odor discrimination within that group.

4.4 Excitatory local neurons

In the proposed model, ELNs had lateral excitation to PNs in the glomeruli that were not activated by an odor. As a result, the PN response to the odor was broadened compared to ORN activation (Fig. 6). Such response broadening has been observed previously (Hallem and Carlson 2006; Bhandawat et al. 2007; Olsen et al. 2007; Shang et al. 2007; Silbering and Galizia 2007; Kazama and Wilson 2009; Huang et al. 2010; Shlizerman et al. 2014), but its function remains unclear. Note that, although PLNs also exhibited lateral inhibition to glomeruli that were not activated by the odor, this inhibition occurred presynaptically in the ORN-to-PN synapses and did not prevent ELNs from activating downstream PNs.

4.5 Same odor with different concentrations

One challenging issue in modeling of olfactory system is how different concentrations of one odor can be recognized as the same odor rather than different odors. Although our model does not consider this issue, it will be addressed in the next developmental stage of the model. One solution is to implement normalization of the PN responses(Olsen et al. 2010). This can be partially achieved by including pan-glomerulus passive LNs, which integrate inputs from all ORNs. With proper tuning and selection of synapse models, the activity levels of this type of LNs can roughly represent the length of a PN response vector, allowing the LNs to perform normalization by suppression PN activities. However, it reminds to be investigated whether such a normalization mechanism affects other functions exhibited by our model.

In conclusion, the present study is significant in several aspects: (1) the model explains how stimulus-frequency dependent responses are produced by short-term depression, (2) the model indicates that the inhomogeneous responses to a GABA antagonist is a side-effect of the presynaptic inhibition, as resulted from the requirements of odor sensitivity, and (3) the model demonstrated that odor identity discrimination is correlated with the innervation pattern of a certain local neuron type.

Acknowledgements The work was supported by the Ministry of Science and Technology grants 101-2311-B-007-008-MY3, 107-2218-E007-033, and by the Higher Education Sprout Project funded by the Ministry of Science and Technology and Ministry of Education in Taiwan.

Compliance with ethical standards

Conflict of interest The authors declare that they have no conflict of interest.

References

Abbott, L. F., Varela, J. A., Sen, K., & Nelson, S. B. (1997). Synaptic depression and cortical gain control. *Science, 275*, 221–224.

Assisi, C., Stopfer, M., & Bazhenov, M. (2012). Excitatory local interneurons enhance tuning of sensory information. *PLoS Computational Biology, 8*, e1002563.

Bhandawat, V., Olsen, S. R., Gouwens, N. W., Schlief, M. L., & Wilson, R. I. (2007). Sensory processing in the drosophila antennal lobe increases the reliability and Separability of ensemble odor representations. *Nature Neuroscience, 10*, 1474–1482.

Chou, Y.-H., Spletter, M. L., Yaksi, E., Leong, J. C. S., Wilson, R. I., & Luo, L. (2010). Diversity and wiring variability of olfactory local interneurons in the drosophila antennal lobe. *Nature Neuroscience, 13*, 439–449.

TA Cleland, C Linster (2012) On-center/inhibitory-surround Decorrelation via Intraglomerular inhibition in the olfactory bulb glomerular layer. *Frontiers in Integrative Neuroscience 6*. Available at: http://www.frontiersin.org/Journal/10.3389/fnint.2012.00005/full [Accessed May 26, 2014].

Cleland, T. A., & Sethupathy, P. (2006). Non-topographical contrast enhancement in the olfactory bulb. *BMC Neuroscience, 7*, 7.

de Bruyne, M., Clyne, P. J., & Carlson, J. R. (1999a). Odor coding in a model olfactory organ: The drosophila maxillary palp. *The Journal of Neuroscience, 19*, 4520–4532.

de Bruyne, M., Clyne, P. J., & Carlson, J. R. (1999b). Odor coding in a model olfactory organ: The drosophila maxillary palp. *The Journal of Neuroscience, 19*, 4520–4532.

de Bruyne, M., Foster, K., & Carlson, J. R. (2001). Odor coding in the drosophila antenna. *Neuron, 30*, 537–552.

Hallem, E. A., & Carlson, J. R. (2006). Coding of odors by a receptor repertoire. *Cell, 125*, 143–160.

Hempel, C. M., Hartman, K. H., Wang, X.-J., Turrigiano, G. G., & Nelson, S. B. (2000). Multiple forms of short-term plasticity at excitatory synapses in rat medial prefrontal cortex. *Journal of Neurophysiology, 83*, 3031–3041.

Huang, J., Zhang, W., Qiao, W., Hu, A., & Wang, Z. (2010). Functional connectivity and selective odor responses of excitatory local interneurons in drosophila antennal lobe. *Neuron, 67*, 1021–1033.

Huston, S. J., Stopfer, M., Cassenaer, S., Aldworth, Z. N., & Laurent, G. (2015). Neural encoding of odors during active sampling and in turbulent plumes. *Neuron, 88*, 403–418.

Jefferis, G. S., Marin, E. C., Stocker, R. F., & Luo, L. (2001). Target neuron prespecification in the olfactory map of drosophila. *Nature, 414*, 204–208.

Kazama, H., & Wilson, R. I. (2008). Homeostatic matching and nonlinear amplification at identified central synapses. *Neuron, 58*, 401–413.

Kazama, H., & Wilson, R. I. (2009). Origins of correlated activity in an olfactory circuit. *Nature Neuroscience, 12*, 1136–1144.

Linster, C., & Cleland, T. A. (2010). Decorrelation of odor representations via spike timing dependent plasticity. *Frontiers in Computational Neuroscience, 4*, 157.

Murlis, J., Elkinton, J. S., & Carde, R. T. (1992). Odor plumes and how insects use them. *Annual Review of Entomology, 37*, 505–532.

Nagel, K. I., & Wilson, R. I. (2016). Mechanisms underlying population response dynamics in inhibitory interneurons of the drosophila antennal lobe. *The Journal of Neuroscience, 36*, 4325–4338.

Nagel, K. I., Hong, E. J., & Wilson, R. I. (2015). Synaptic and circuit mechanisms promoting broadband transmission of olfactory stimulus dynamics. *Nature Neuroscience, 18*, 56–65.

Ohliger-Frerking, P., Wiebe, S. P., Staubli, U., & Frerking, M. (2003). GABAB receptor-mediated presynaptic inhibition has history-dependent effects on synaptic transmission during physiologically relevant spike trains. *The Journal of Neuroscience, 23*, 4809–4814.

Okada, R., Awasaki, T., & Ito, K. (2009). Gamma-aminobutyric acid (GABA)-mediated neural connections in the drosophila antennal lobe. *The Journal of Comparative Neurology, 514*, 74–91.

Olsen, S. R., & Wilson, R. I. (2008). Lateral presynaptic inhibition mediates gain control in an olfactory circuit. *Nature, 452*, 956–960.

Olsen, S. R., Bhandawat, V., & Wilson, R. I. (2007). Excitatory interactions between olfactory processing channels in the drosophila antennal lobe. *Neuron, 54*, 89–103.

Olsen, S. R., Bhandawat, V., & Wilson, R. I. (2010). Divisive normalization in olfactory population codes. *Neuron, 66*, 287–299.

Park, I. M., Bobkov, Y. V., Ache, B. W., & Príncipe, J. C. (2014). Intermittency coding in the primary olfactory system: A neural substrate for olfactory scene analysis. *The Journal of Neuroscience, 34*, 941–952.

Park, I. J., Hein, A. M., Bobkov, Y. V., Reidenbach, M. A., Ache, B. W., & Principe, J. C. (2016). Neurally encoding time for olfactory navigation. *PLoS Computational Biology, 12*, e1004682.

Raccuglia, D., McCurdy, L. Y., Demir, M., Gorur-Shandilya, S., Kunst, M., Emonet, T., & Nitabach, M. N. (2016). Presynaptic GABA receptors mediate temporal contrast enhancement in drosophila olfactory sensory neurons and modulate odor-driven behavioral kinetics. *eNeuro, 3*, 0080–16.2016.

Rangan, A. V. (2012). Functional roles for synaptic-depression within a model of the Fly antennal lobe. *PLoS Computational Biology, 8*, e1002622.

Reisenman, C. E., Dacks, A. M., & Hildebrand, J. G. (2011). Local interneuron diversity in the primary olfactory center of the moth Manduca sexta. *Journal of Comparative Physiology. A, Neuroethology, Sensory, Neural, and Behavioral Physiology, 197*, 653–665.

Riffell, J. A., Shlizerman, E., Sanders, E., Abrell, L., Medina, B., Hinterwirth, A. J., & Kutz, J. N. (2014). Flower discrimination by pollinators in a dynamic chemical environment. *Science, 344*, 1515–1518.

Seki, Y., Rybak, J., Wicher, D., Sachse, S., & Hansson, B. S. (2010). Physiological and morphological characterization of local interneurons in the drosophila antennal lobe. *Journal of Neurophysiology, 104*, 1007–1019.

Shang, Y., Claridge-Chang, A., Sjulson, L., Pypaert, M., & Miesenböck, G. (2007). Excitatory local circuits and their implications for olfactory processing in the Fly antennal lobe. *Cell, 128*, 601–612.

Shlizerman, E., Riffell, J. A., & Kutz, J. N. (2014). Data-driven inference of network connectivity for modeling the dynamics of neural codes in the insect antennal lobe. *Frontiers in Computational Neuroscience, 8*, 70.

Silbering, A. F., & Galizia, C. G. (2007). Processing of odor mixtures in the drosophila antennal lobe reveals both global inhibition and glomerulus-specific interactions. *The Journal of Neuroscience, 27*, 11966–11977.

Stocker, R. F., Lienhard, M. C., Borst, A., & Fischbach, K. F. (1990). Neuronal architecture of the antennal lobe in Drosophila melanogaster. *Cell and Tissue Research, 262*, 9–34.

Sun, H., Ma, C. L., Kelly, J. B., & Wu, S. H. (2006). GABAB receptor-mediated presynaptic inhibition of glutamatergic transmission in the inferior colliculus. *Neuroscience Letters, 399*, 151–156.

Varela, J. A., Sen, K., Gibson, J., Fost, J., Abbott, L. F., & Nelson, S. B. (1997). A quantitative description of short-term plasticity at excitatory synapses in layer 2/3 of rat primary visual cortex. *The Journal of Neuroscience, 17*, 7926–7940.

Wang, X.-J. (1999). Fast burst firing and short-term synaptic plasticity: A model of neocortical chattering neurons. *Neuroscience, 89*, 347–362.

Wang, J. W. (2012). Presynaptic modulation of early olfactory processing in drosophila. *Developmental Neurobiology, 72*, 87–99.

Wilson, R. I. (2013). Early olfactory processing in drosophila: Mechanisms and principles. *Annual Review of Neuroscience, 36*, 217–241.

Wu, L. G., & Saggau, P. (1994). Presynaptic calcium is increased during normal synaptic transmission and paired-pulse facilitation, but not in long-term potentiation in area CA1 of hippocampus. *The Journal of Neuroscience, 14*, 645–654.

Wu, L.-G., & Saggau, P. (1997). Presynaptic inhibition of elicited neurotransmitter release. *Trends in Neurosciences, 20*, 204–212.

Yu, Y., Migliore, M., Hines, M. L., & Shepherd, G. M. (2014). Sparse coding and lateral inhibition arising from balanced and unbalanced dendrodendritic excitation and inhibition. *The Journal of Neuroscience, 34*, 13701–13713.